Title

Nanostructured Graphene Oxide Composite Membranes with Ultrapermeability and Mechanical Robustness

Journal

Nano Letters, 20(4)

ISSN

1530-6984

Authors

Xue, Shuangmei
Ji, Chenhao
Kowal, Matthew D
et al.

Publication Date

2020-04-08

DOI

10.1021/acs.nanolett.9b03780

Peer reviewed

NANO LETTERS

pubs.acs.org/NanoLett Letter

Nanostructured Graphene Oxide Composite Membranes with Ultrapermeability and Mechanical Robustness

Shuangmei Xue,[‡] Chenhao Ji,[‡] Matthew D. Kowal, Jenna C. Molas, Cheng-Wei Lin, Brian T. McVerry, Christopher L. Turner, Wai H. Mak, Mackenzie Anderson, Mit Muni, Eric M. V. Hoek, Zhen-Liang Xu, and Richard B. Kaner*

Cite This: https://dx.doi.org/10.1021/acs.nanolett.9b03780 Read Online

ACCESS | Metrics & More | Article Recommendations | Supporting Information

ABSTRACT: Graphene oxide (GO) membranes have great potential for separation applications due to their low-friction water permeation combined with unique molecular sieving ability. However, the practical use of deposited GO membranes is limited by the inferior mechanical robustness of the membrane composite structure derived from conventional deposition methods. Here, we report a nanostructured GO membrane that possesses great permeability and mechanical robustness. This composite membrane consists of an ultrathin selective GO nanofilm (as low as 32 nm thick) and a postsynthesized macroporous support layer that exhibits excellent stability in water and under practical permeability testing. By utilizing thin-film lift off (T-FLO) to fabricate membranes with precise optimizations in both selective and support layers, unprecedented water permeability (47 $L \cdot m^{-2} \cdot hr^{-1} \cdot bar^{-1}$) and high retention (>98% of solutes with hydrated radii larger than 4.9 Å) were obtained.

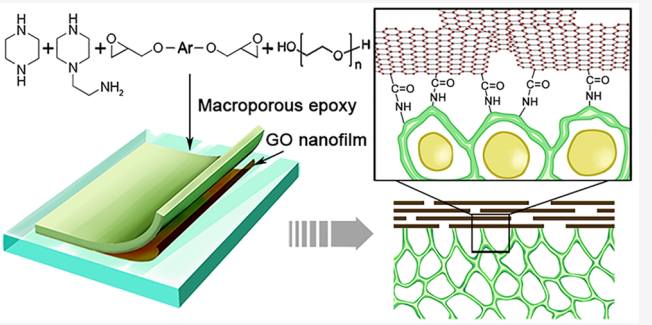

KEYWORDS: *graphene oxide, nanostructure, molecular sieving, thin-film composite, mechanical robustness, membrane separation*

INTRODUCTION

Selectively permeable membranes offer efficient, environmentally friendly separation processes with versatile applications in water purification and clean energy production.[1] Thin-film composite membranes are designed to maximize permeability and minimize cost and are tailored for use in nanofiltration, gas separation, and desalination. The ideal structure of a highly permeable membrane is a defect-free, dense, ultrathin selective film reinforced by a porous support layer that offers mechanical strength with low permeation resistance.[2−4] To improve current state-of-the-art thin-film membranes, researchers have recently envisaged the use of 2D nanomaterials to improve the transport and material properties of membranes.[5,6] Owing to the distinct laminar structure and tunable physicochemical characteristics, graphene-based nanomaterials show great potential for water purification.[7−13] Graphene is a one atom thick two-dimensional sp^2 carbon lattice that possesses strong mechanical properties, chemical tolerance, and an extremely large surface area.[14,15] In its oxidized form, graphene oxide (GO) has become a well-studied nano-sized building block for use as the selective layer in separation membranes.[16−18] Previous studies have indicated that GO laminates provide ultrafast transport of water through low-friction flow 2D capillaries for a monolayer of water.[19,20]

Despite the exceptional transport properties of GO laminates, the fabrication and practical application of thin-film composite membranes containing a defect-free GO laminate active layer is cumbersome. Current methods for preparing ultrathin GO membranes involve flow-directed filtration,[21] film coating,[22] and layer-by-layer assembly.[14] Although the interaction of GO laminates can be improved by partial reduction as well as ionic or organic cross-linking,[18,19] current methods of depositing GO laminates directly on previously fabricated membranes still face the great challenge that the GO selective layer will readily detach from the substrate under hydraulic conditions.[23−25] However, almost no effort has been made in overcoming the fragility problem of GO composite membranes, which limits the potential for further industrialization. For the membranes with assembled GO selective layers, new fabrication techniques are needed that both increase the mechanical robustness of the composite structure (adhesion between the GO and the support layer) and enable large-scale fabrication of GO laminate composite membranes.

Received: September 12, 2019
Revised: February 10, 2020
Published: February 14, 2020

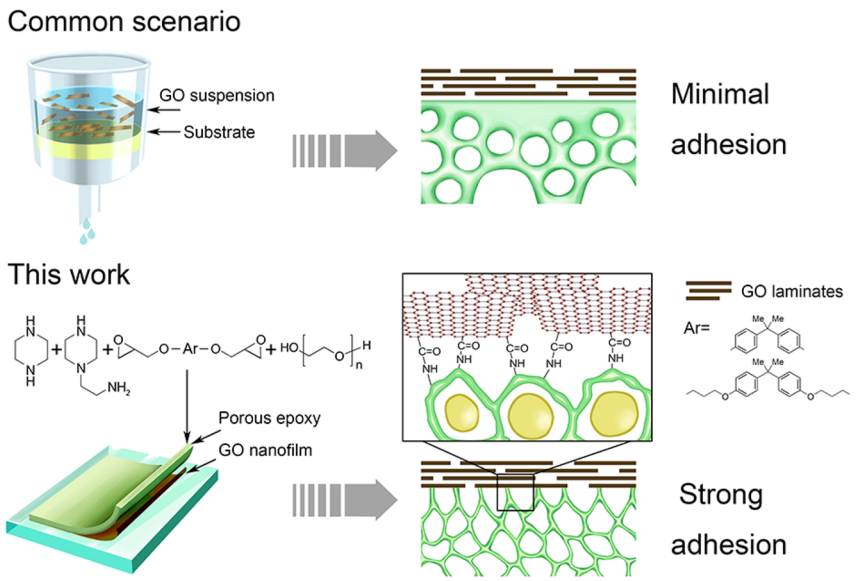

Figure 1. Schematic of a nanostructured graphene oxide (T-FLO-GO) composite membrane. Common scenario: the deposition of a GO film by filtering a GO suspension onto a substrate (minimum adhesion in the composite structure). This work: postpolymerizing an epoxy layer with percolating porous structure onto a GO nanofilm results in strong adhesion within the composite structure.

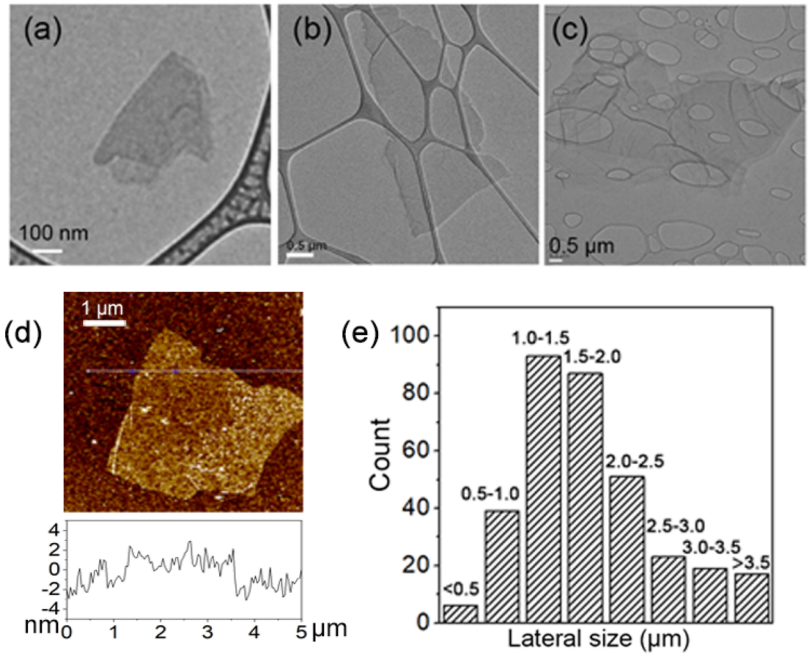

Figure 2. GO flake size distribution. TEM images of (a) a small GO flake, (b) a medium GO flake, and (c) a large GO flake. (d) AFM topographic images of GO flakes used for the fabrication of GO membranes. (e) The flake size distribution based on TEM analysis. The flake sizes were estimated by taking the square root of the area of each flake measured with ImageJ software.

In our previous work, McVerry et al.[26] have developed a novel thin-film lift off (T-FLO) technique that enables the fabrication of asymmetric composite membranes with new polymers. Here, we employ T-FLO to make mechanically robust nanostructured membranes using large-area and well-aligned GO nanofilms as the selective layer to fully exploit the mass transfer properties of GO. With precise control over GO film thickness and chemical composition of the support layer, the optimal GO membrane provides an ultrafast water permeance of 47 $L{\cdot}m^{-2}{\cdot}hr^{-1}{\cdot}bar^{-1}$ and excellent retention of solutes with hydrated radii larger than 4.9 Å. The improved interactions between the GO laminate and the GO−epoxy interface endow the nanostructured GO membrane with much improved mechanical stability compared to conventionally deposited GO membranes. This work presents the first practical and industrially scalable composite membrane using neat GO as the selective layer.

RESULTS AND DISCUSSION

The robust GO membranes are obtained by postsynthesizing a macroporous epoxy layer on a readily cast GO film (Figures 1 and S1). In order to fabricate large-area aligned GO films, a GO dispersion is blade coated onto a nonadherent surface.[22] The GO synthesized in our lab possesses an average lateral size

https://dx.doi.org/10.1021/acs.nanolett.9b03780
Nano Lett. XXXX, XXX, XXX−XXX

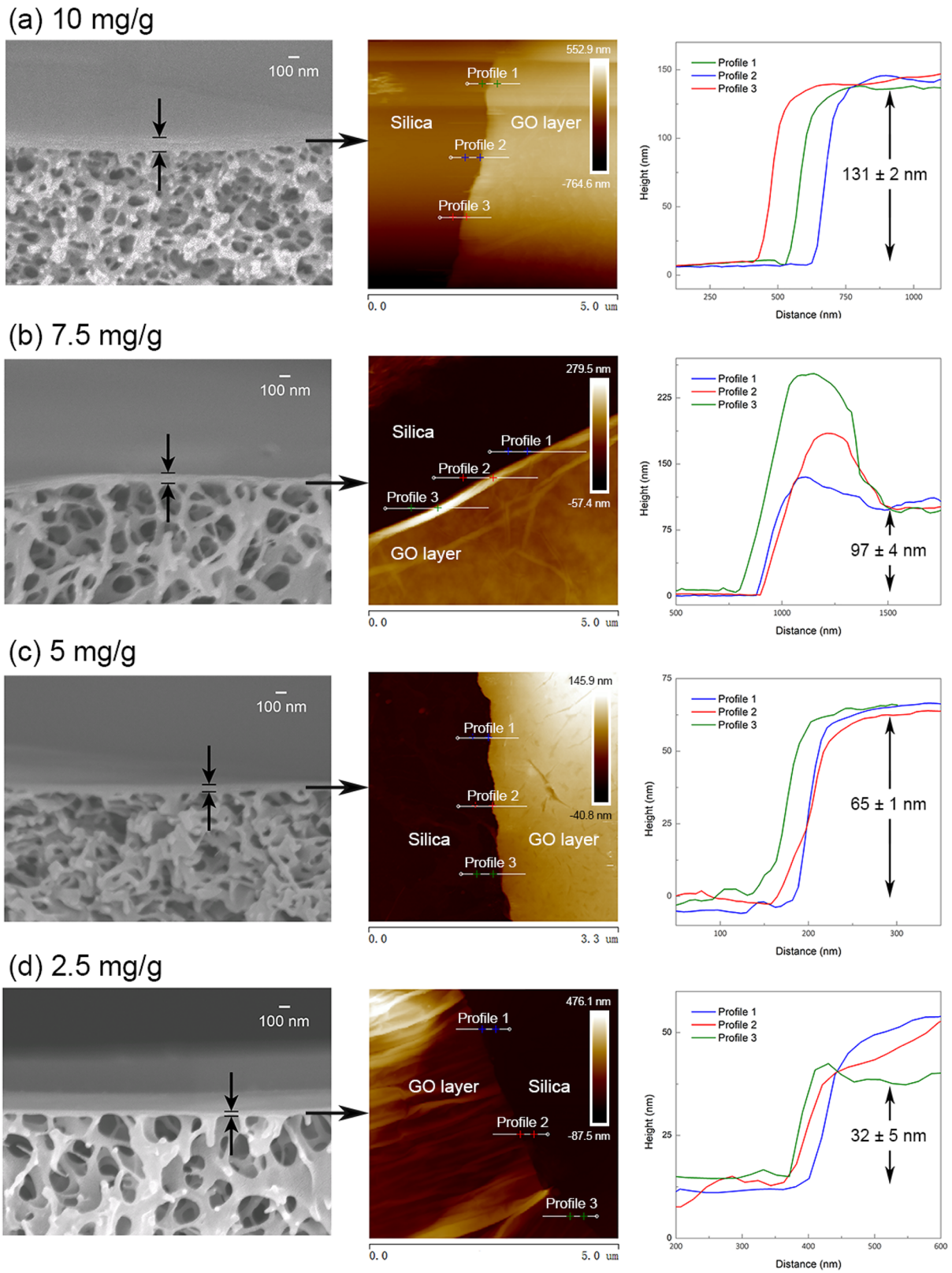

Figure 3. T-FLO-GO membranes with different GO layer thicknesses. The SEM cross-sectional morphology and AFM film thicknesses as a function of the concentrations of GO used in the casting solution: (a) 10, (b) 7.5, (c) 5, and (d) 2.5 mg/g. No significant change in the GO layer thickness is observed before and after the macroporous support layer is synthesized. All membranes were prepared with support layers containing a PIP:APIP diamine molar ratio of 9:1.

of ∼1.0−2.0 μm according to statistical analyses of transmission electron microscopy (TEM) images (Figure 2). The sedimentation of GO sheets is influenced by two factors—the shear alignment created by the blade casting and the thickness dependent solvent evaporation mechanical behavior.[27,28] When GO membranes are deposited on porous substrates,

https://dx.doi.org/10.1021/acs.nanolett.9b03780
Nano Lett. XXXX, XXX, XXX−XXX

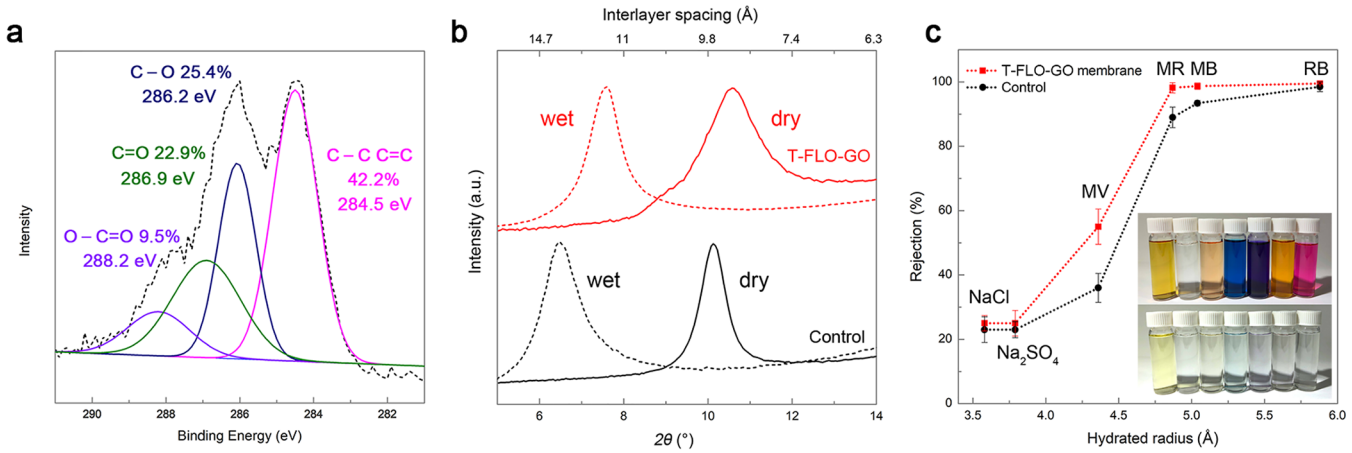

Figure 4. (a) XPS C 1s of the top surface of aT-FLO-GO membrane containing a 32 nm thick nanofilm. (b) X-ray diffraction showing shifts of the (001) peak due to the swelling of the selective layer in the GO membranes after immersion in water. (c) Molecular sieving ability as a function of solute hydrated radii for NaCl; Na_2SO_4; MV, methyl viologen (4.36 Å); MR, methyl red (4.87 Å); MB, methylene blue (5.04 Å); and RB, rose bengal (5.88 Å). Inset: photos of the feed and permeate of the aqueous solutions. The small-weight organics used are CG, chrysoidine G (248.71 Da), CV, crystal violet (407.98 Da), XO, xylenol orange (672.67 Da), MV (257.16 Da), MR (269.30 Da), MB (319.85 Da), and RB (973.67 Da). The hydrated radii and molecular weight of the dyes are listed in Table S2.

small inhomogeneities on the surface of the base layer will initiate wrinkles in the GO films and influence the resulting membrane surfaces (Figure S2). The formation of a flat and well-aligned GO film can be obtained by controlling the deposition speed and film thickness. To form defect-free ultrathin GO nanofilms, GO sheets in a dilute solution were deposited onto glass, which forms a smooth and highly ordered 2D capillary network for the GO membranes (Figure S3a).[29] Sheet-like structures observed by atomic force microscopy (AFM) reveal that the films are made from the horizontal deposition of GO flakes with a root-mean-square roughness as low as 4.02 ± 0.26 nm (Figure S3b). As a result, a compact layer with a high degree of horizontal sheet orientation is achievable with the blade-casting method.

Furthermore, the GO film thicknesses can be readily controlled by modifying the concentrations of the casting solution. A series of aqueous GO solutions (2.5, 5, 7.5, and 10 mg/g) were cast onto silicon wafers, and the resulting film thicknesses range from 32 to 131 nm (Figure 3). Film thickness measurements were conducted using AFM after the GO films were deposited on the wafers and dried. After AFM analysis, epoxy precursor solutions can then be cast directly onto the GO films and cured for 6 h in the oven at 120 °C to form the composite. The composite containing the additive is then placed in a water bath for the formation of a percolating epoxy layer and dried for SEM analysis. The thicknesses of the GO layer in the T-FLO-GO membranes correspond to the GO films cast on the silicon wafers, indicating that the polymerization of the macroporous epoxy does not cause significant changes in the thickness of the GO layer.

Random stacking of individual GO sheets and defects in the GO lattice are known to generate pinholes in GO films.[30,31] When T-FLO-GO membranes are made from a very dilute 1 mg/g GO solution, a defect-free thin film cannot be produced, and tiny pores are observed in SEM from the epoxy support (Figure S4). This occurs because the GO sheets do not form an effective barrier between the underlying substrate and epoxy resin. Membranes with a GO film thickness below the critical thickness exhibit no molecular cutoff capability for solutes with hydrated radii less than 5.88 Å. Benefiting from the fine interlayer alignment, the minimum concentration needed to fabricate a T-FLO-GO membrane with an intact selective layer is 2.5 mg/g.

The macroporous epoxy support layer is formed by polymerization-induced phase separation using four epoxy-based monomers with distinct characteristics. The copolymer was polymerized *in situ* in the presence of a water-soluble porogen and formed into an ideal percolating structure after the porogen was removed via solvent exchange. To optimize the composite structure of membranes, a quaternary monomer system containing two bisphenol A type diepoxides and two diamines was designed for a highly controllable porous structure (Figure S5). The porogen, poly(ethylene glycol) M_n = 400 (PEG_{400}), was selected for its good compatibility with the precursor solution. During the polymerization, the porogen is trapped in the newly formed epoxy network. The resulting membrane is placed into a bath of water to remove the porogen and form the macroporous layer.[26]

To investigate the effect of the epoxy curing on the GO film, the membranes were analyzed using X-ray photoelectron spectroscopy (XPS). Abundant oxygen containing groups are observed in the XPS C 1s spectra (Figure 4a). Upon comparison of the T-FLO-GO membrane surface with pristine and heat-treated (120 °C, 6 h) GO films in Figure S6, the C/O ratio has increased slightly, and the intensity of the C=O peak on the membrane surface has decreased after treatment, indicating that the GO layer in the membrane experienced partial reduction but with only minimal losses of oxygen containing groups (Figure S7).[32] This is also consistent with the X-ray diffraction (XRD) patterns of T-FLO-GO membranes where there is no observation of fully reduced graphite peaks (002, 2θ around 26°, Figure S8). Furthermore, the variation in epoxy chemical structure does not interfere with the alignment of the GO laminates, because no shift of the GO (001) peak is observed when the substrate compositions are changed.

Mechanical robustness is a major concern for GO membranes and must be addressed for industrially applicable membrane separations. Freestanding GO films that underwent heat treatment (120 °C, 6 h) exhibited higher stability

https://dx.doi.org/10.1021/acs.nanolett.9b03780
Nano Lett. XXXX, XXX, XXX−XXX

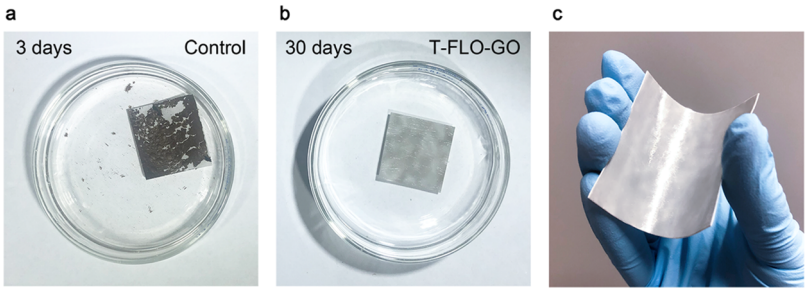

Figure 5. Mechanically robust T-FLO-GO membranes. (a) Photo of a control in water for 3 days. The control was air-dried before being placed into water. (b) Photo of a T-FLO-GO membrane immersed in water for 30 days. (c) Photo of a bent T-FLO-GO membrane with a 32 nm thick GO layer and a 9:1 diamine ratio.

compared to a pristine GO film (Figure S9a). Interactions such as $\pi-\pi$ stacking and hydrogen bonding help to keep the GO laminates stable; however, the stability of the GO/substrate interface is quite limited based on conventional deposition methods. The GO films of deposited GO membranes can readily detach from their support membranes after being kept in water for only 3 days (Figure 5a). In contrast, for the T-FLO-GO membranes in which the GO selective layer underwent the same heat treatment, covalent bonds to the macroporous support layer form, meaning that the mechanical robustness of a T-FLO-GO membrane is significantly enhanced in both the GO laminates and the composite structure. As a result, after being kept in water for 30 days, no obvious change in the composite structure was observed (Figure 5b,c). The SEM morphology and molecular sieving performance also demonstrate that the T-FLO-GO membranes keep their integrity after being placed in water for 30 days (Figure S9b–d). Uniaxial tensile strength was employed to evaluate the interlayer binding strength of the GO membranes (Figure S10). Similar to the phenomenon observed under the wet condition, the poor mechanical robustness of a dry deposited GO membrane was mainly attributed to the inferior adhesion between GO and the support layer as they separated under a stress of 0.68 MPa. However, the interlayer binding strength in a dry T-FLO-GO is at least stronger than the adhesion between the glass holder and a commercial adhesive of ~1.07 MPa. We further analyzed the mechanical properties of a wet membrane by operating membranes installed inversely in a dead-end cell. If decomposition or defects are generated in the selective GO layer, then the flux of the T-FLO-GO membrane will be unable to increase linearly with the operating pressure (Figure S11a,b). The permeation flux of the membrane was stable when operated across a pressure range of 15–300 psi, demonstrating that the membrane can adapt to a wide variety of operating conditions. Additionally, the T-FLO-GO membrane maintained its excellent performance after continuous operation for 24 h (Figure S11c). The stable separation performance under different pressures and long-time operation indicates that these membranes could be used for practical applications.

To investigate adhesion between the GO layer and porous epoxy layer, an epoxy/GO composite was made by *in situ* polymerization of a mixture of monomers and freeze-dried GO. The formation of amide bonds was observed by ATR-FTIR (Figure S12) indicating that the monomers can bond to the carboxyl groups on the GO sheets. Note that the GO films only underwent heat treatment during the curing process. Therefore, adhesions between the GO and the support layer leading to a robust composite structure are obtained by the covalent bonds formed at the GO–epoxy interface.

The atomic-scale sieving capability of the assembled GO laminate is determined by three factors: the interlayer channels, the functional groups, and the pores/defects on the carbon lattice.[32−35] In regards to deposited GO membranes for water purification, the first two factors provide synergistic effects and dictate the molecular transport properties.[31,36,37] The interlayer spacing between GO sheets (d-spacing), i.e., the fluid pathways in the deposited GO membranes, is determined by the swelling conditions of GO laminates in a given solvent. The pathways for water permeation in the assembled GO film are the interlayer channels of the GO laminates, and their steric effects are determined by the d-spacing between the GO sheets. The change in d-spacing due to swelling of GO layers in the T-FLO-GO membrane versus the control (conventionally deposited GO membrane) was examined using XRD (Figure 4b). Due to the heat curing for synthesizing the epoxy layer, the T-FLO-GO membranes undergo less swelling in water, observed by the GO (001) peak shift, compared to the pure GO film, indicating a narrower interlayer spacing when swelled.

To probe the molecular sieving properties of the GO membranes, we conducted pressure-driven filtrations of aqueous solutions of several salts and organic dyes. The T-FLO-GO membrane can block over 98.2 ± 1.6% of all solutes with hydrated radii larger than 4.9 Å (Figure 4c). The membrane rejection capability is governed by the d-spacing of the GO laminates and therefore cannot reject ions with a hydrated diameter much smaller than the d-spacing between the GO laminates under wet conditions. Due to the change in the d-spacing of the laminates when swelled, the T-FLO-GO membranes have a slightly higher rejection of organic dyes with hydrated sizes from 4.36 to 5.04 Å compared to the control GO membrane. Furthermore, we performed the filtration test using organic solutes with different molecular weights. Images of the feed and permeate solutions are shown in the inset to Figure 4c. A sharp molecular weight cutoff of ~270 Da was observed for the T-FLO-GO membranes (Figure S13). More importantly, the control membrane (made from filtration of a 30 mg/L GO aqueous suspension on a polyether sulfone ultrafiltration membrane) showed no rejection of small molecules when the GO film thickness was less than 131 nm.

Ultrahigh permeance to fluids may occur in thin-film composite membranes with decreased transfer resistance, made possible by the optimization of both the selective and support layers. To further evaluate the permeability of the T-FLO-GO membranes, we performed dead-end pressure filtration with water as a function of the epoxy layer structure

https://dx.doi.org/10.1021/acs.nanolett.9b03780
Nano Lett. XXXX, XXX, XXX−XXX

and the GO layer thickness. The separation performance of membranes with thicknesses of 32, 65, 97, and 131 nm were tested (Figure 6c). Exponential improvement in the permeability is observed when decreasing the GO thickness, which is consistent with the permeance reported for ultrathin filtration deposited GO membranes.[30,38] The membranes with thicknesses around 32−131 nm all possess defect-free GO layers and thus have relatively constant rejection as the GO film thickness decreases.

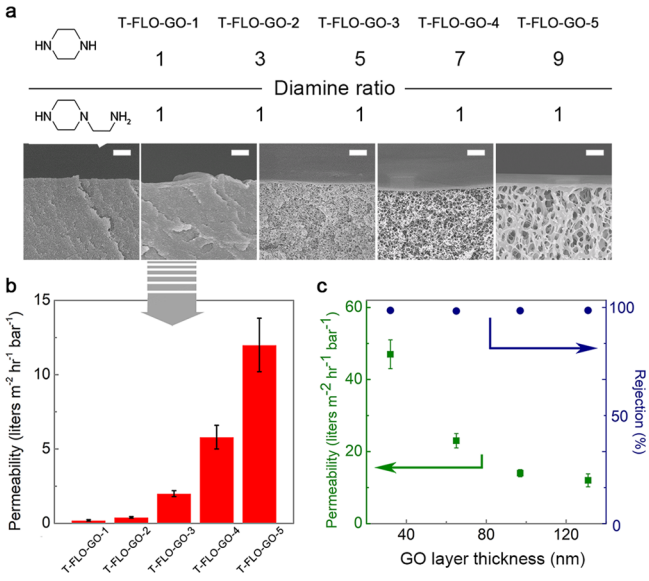

Figure 6. Permeability through T-FLO-GO membranes with tunable composite structures. (a) Cross section of membranes with epoxy layers made from a series of different diamine ratios. Scale bar 1 μm. (b) Permeability as a function of different epoxy formulas (all of the membranes have a selective layer made from a 10 mg/g GO solution). (c) Separation performance as a function of the GO layer thickness (the thicknesses used are 32, 65, 97, and 131 nm).

The flexibility and degree of cross-linking of the polymer chains were varied by changing the ratio of diepoxides and diamines. Combinations of two diepoxides, bisphenol A diglycidyl ether (BADGE) and bisphenol A propoxylate diglycidyl ether (BAPDGE), were used to alter the rigidity of the resultant polymer chain. Furthermore, different diamines, piperazine and 1-(2-aminoethyl) piperazine, were used to modify the amount of cross-linking within the epoxy network. Compared to a cured epoxy with only piperazine (PIP) as the diamine, the primary amine group in 1-(2-aminoethyl) piperazine (APIP) leads to a more cross-linked structure. The degree of cross-linking and chain flexibility influences the amount of additive held within the epoxy matrix during phase separation, thus varying the pore size of the resulting support layer. The increasing opacity in the support layer indicates the enhanced scattering of light from the enlarged pores (Figure S14). Considering that a primarily linear chain structure lacks sufficient anchor points to peel off a defect-free GO nanofilm, the maximum PIP:APIP diamine molar ratio applied was 9:1.

The influence of the diamine ratio on the epoxy porous structure (all of the membranes have a selective GO layer of ∼130 nm thick) is shown in Figure 6a, and their resultant permeability is exhibited in Figure 6b. A dense epoxy support in T-FLO-GO-1 causes high resistance to permeability and dominates the membrane flux. However, when the 131 nm thick GO layer is coupled with a macroporous epoxy layer (T-FLO-GO-5), a flux of 12.0 ± 1.8 L·m^{-2}·hr^{-1}·bar^{-1} was obtained. This permeability demonstrates a 2 orders of magnitude improvement compared with T-FLO-GO-1 owing to faster water transport in larger pores. For the most permeable GO membrane, a 32 nm GO laminate with epoxy made from a diamine ratio of 9:1 (which has the largest pores) endows the resulting T-FLO-GO membrane with an ideal flux of 47.2 ± 4.9 L·m^{-2}·hr^{-1}·bar^{-1} and a retention of >98.2% for solutes with hydrated radii greater than 4.9 Å. More importantly, the separation performance of T-FLO-GO membranes is compared with typical performance of as-deposited GO-based membranes reported in the literature (Figure S15). Distinct from known GO-based membranes with GO laminates deposited on previously fabricated substrates, our GO membranes can be more readily tuned in their composite structure, thus allowing for both excellent permeance and strict molecular sieving ability.

CONCLUSION

In this contribution, we employ T-FLO to fabricate mechanically robust nanostructured GO membranes that possess high water permeability and good rejection of organic small molecules. By postpolymerizing a macroporous epoxy on the blade-cast GO nanofilm, improved interactions between the GO laminate and the GO−epoxy interface are obtained. The composite membrane exhibits excellent stability in water and under practical permeability testing. This solves the main drawback of conventionally deposited GO membranes and allows optimizations of both the ultrathin GO layer and the porous layer. With a pinhole-free GO nanofilm (as thin as 32 nm thick) and a macroporous epoxy layer, the highest performing nanostructure GO membrane exhibited unprecedented water permeance up to 47 L·m^{-2}·hr^{-1}·bar^{-1} and high retention (>98% of solutes with hydrated radii larger than 4.9 Å). We believe these nanostructured GO membranes are ideal candidates for industrially feasible membrane-based separation with proper optimization and scaling.

EXPERIMENTAL SECTION

Materials. Two diepoxides and two diamines (Sigma-Aldrich) were used as the epoxy precursors: bisphenol A diglycidyl ether (BADGE), bisphenol A propoxylate diglycidyl ether (BAPDGE), piperazine (PIP, 99%), and 1-(2-aminoethyl) piperazine (APIP, 99%), respectively. The doctor blade (Gardco) used for casting the ultrathin active layer has a 16 cm width and 0.3 MIL (7.62 μm) horizontal spacing. A nonwoven fabric (Resin Flow Media, Technical Fibre Products) was used for membrane fabrication.

Graphite (Bay Carbon, SP-1-325) and other chemicals used for the synthesis of graphene oxide (GO) including concentrated sulfuric acid (Fisher Scientific), hydrochloric acid (Sigma-Aldrich), hydrogen peroxide solution (30% (w/w), Sigma-Aldrich), potassium persulfate (Alfa Aesar), phosphorus pentoxide (>98%, Fluka), and potassium permanganate (Acros) were used as received.

PES UF membranes (Synder Filtration) with a molecular weight cutoff of 30 000 Da were used as the support layer to prepare conventional GO (control) membranes. Acetone, ethanol, and isopropanol (Sigma-Aldrich) were all reagent grade and used as received. The salts used to test membrane rejection (sodium chloride and sodium sulfate, Sigma-Aldrich)

https://dx.doi.org/10.1021/acs.nanolett.9b03780
Nano Lett. XXXX, XXX, XXX−XXX

were used as received. The organic dyes used to determine the molecular-weight-cutoff: methyl viologen dichloride hydrate (98%), methyl red, methylene blue (≥82%), and rose bengal (95%) were obtained from Sigma-Aldrich and used as received.

Preparation of Graphene Oxide. Graphene oxide was synthesized by a two-step process: preoxidation followed by a modified Hummers method. In the first step, concentrated sulfuric acid (125 mL) was heated to 90 °C. Potassium sulfate (25 g), phosphorus pentoxide (25 g), and graphite (30 g) were then added and stirred for 4.5 h under constant temperature (90 °C). After the reaction, the suspension was allowed to cool to room temperature, followed by dilution with 6 L of deionized (DI) water. The mixture was then vacuum filtered and rinsed to a neutral pH (pH = 7). The resultant preoxidized graphite was dried overnight. The second step involved oxidation using a modified Hummers method. Subsequently, 25 g of preoxidized graphite was added to 1.15 L of concentrated sulfuric acid at 0 °C. Potassium permanganate (150 g) was added slowly into the container, while the temperature was kept below 10 °C. The mixture was allowed to warm up to room temperature and reacted for 4 days. Upon completion, the mixture was poured into 5 kg of crushed ice and diluted to 20 L. Hydrogen peroxide (30%, 300 mL) was added into the mixture. The crude graphene oxide was washed 5 times with a dilute hydrochloric acid solution (5 L, 10%). The mixture was washed 8 times with 5 L of DI water and dialyzed for 2 weeks in a fresh DI water bath. The GO flakes was loaded onto a silicon wafer for the topographic analysis using AFM and dropped onto a copper mesh for observation under TEM.

Blade Casting of GO Film. The ultrathin GO active layer was prepared by solvent evaporation precipitation. A concentrated GO aqueous emulsion (20.02 mg/g) was diluted in a series of concentrations (2.5, 5, 7.5, 10 mg/g) and then ultrasonicated for 5 min. The casting tool used was a bar applicator (GardCo) with a rectangular outlet formed between the blade tip and the substrate, through which the movable blade spreads the GO dispersion onto the substrate. The bar applicator has a gap size of 0.3 MIL (7.62 μm), which can produce a wet film of ∼0.3 MIL. Typically to prepare a GO film, 2 mL of a homogeneous GO dispersion (with different GO concentrations) was placed along the edge of the glass plate using a pipet, and then, the GO solution was pushed by the blade tip of the bar applicator to form the wet GO film. The manual casting speed was controlled to ∼1 cm·s^{-1}, and the extra GO solution was pushed off the glass plate edge to prevent backflow. Subsequently, the liquid film was dried at room temperature (25 °C) to evaporate the water and precipitate the GO film. The GO films loaded on the glass sheets were preserved in a dust-free environment for the subsequent epoxy layer synthesis. The glass plate was thoroughly washed followed by cleaning in concentrated sulfuric acid to remove any impurities. Before the GO film was cast, the glass plate was taken out from the acid bath, rinsed, and neutralized with DI water and then scrubbed with acetone and dried. As demonstrated in some current literature reports, the shear forces during blade casting can help orient the graphene oxide sheets into a dense continuous, uniform film.[3]

Preparation of the Epoxy Precursor. Piperazine (PIP) or 1-(2-aminoethyl) piperazine (APIP) served as the amine source. Bisphenol A diglycidyl ether (BADGE) or bisphenol A propoxylate diglycidyl ether (BAPDGE) were the epoxy sources for the *in situ* polymerization of the porous epoxy. Due to the high viscosity of the precursor solution, the diamines were first carefully weighed and thoroughly mixed before the epoxy monomers were added. Different mass ratios of the diamines with a total mass of 0.4 g were added into 6.50 g of PEG_{400} with 0.50 g of ethanol and vigorously stirred at 60 °C for 30 min. PEG_{400} served as the additive and reaction medium, while the ethanol was added to decrease the viscosity of the solution. After the solution was cooled to room temperature, 1.36 g of BADGE or 0.57 g of BAPDGE were added into the vessel and stirred for another 30 min to make a homogeneous epoxy precursor.

To further investigate the influence of chemical composition on the structure of the support layer, different ratios of the diamines were used to fabricate a series of support layers. The specific formulas are listed in Table S1.

Fabrication of Nanostructured GO Membranes. A piece of nonwoven fabric was measured according to the area of the precast GO film and gently placed on the top of the GO film (supported by a glass plate) to provide mechanical strength and assist the homogeneous spread of the viscous solution. The as-prepared epoxy precursor was cast on one side of the GO film. The glass was tilted, and the solution was allowed to slowly spread along the nonwoven fabric. After the precursor solution soaked into the entire fabric, the glass plate was horizontally placed and transferred into an oven for 6 h at 120 °C. The resultant membrane was cooled overnight and then placed into a water bath for 6 h to remove the additive. After some small areas of adhesion were separated along the edge of the fabric, the whole membrane could be readily lifted off from the glass plate with an intact selective layer. The membrane was then preserved in DI water to completely remove the additive before testing.

Preparation of Conventional GO (Control) Membranes. For better understanding of the sieving ability of the T-FLO-GO membranes, conventional GO membranes were prepared by pressure-assisted filtration of a GO aqueous solution on a commercial PES UF membrane. GO dispersion (50 mL) with a concentration of 30 mg/L was added into a dead-end cell. Commercial PES ultrafiltration membranes were used as the substrate for the filtration under 30 psi. After filtration, the solute solution was added directly into the feed chamber to avoid destruction of the GO layer. The feed and permeate solutions were sampled for further analysis.

Characterizations. The GO composite membranes were visualized by scanning electron microscope (SEM, JEOL, USA) with an accelerating voltage of 5 kV and a current of 9.0 μA. For imaging the cross sections, a strip of membrane was air-dried and freeze-fractured under liquid nitrogen. A layer of platinum was sputtered on the samples for 1 min under 15 mA to reduce charging for obtaining reliable images. The surface topography and thickness of the GO films were evaluated by AFM (Bruker, USA) with a ScanAsyst Air probe. As for the surface topography, a 1 × 1 cm^2 membrane was attached onto a glass slide using double sided tape. For thickness analysis, an edge of the GO film was located, and the height difference between the GO layer and the background was analyzed. The silicon wafer was pretreated in 50 mL of isopropanol and sonicated for 30 min to remove any surface impurities. The AFM results were further analyzed using Nanoscope Analysis for the surface roughness and thicknesses of GO films. The chemical compositions of the GO layers were analyzed by X-ray photoelectron spectroscopy analysis (XPS, Kratos AXIS

https://dx.doi.org/10.1021/acs.nanolett.9b03780
Nano Lett. XXXX, XXX, XXX−XXX

Ultra DLD, USA) and Fourier-transform infrared spectrometer (FT-IR, Jasco FT/IR-6300, USA) under attenuated total reflectance (ATR) mode. Due to the limited content of the GO layer on the whole sample, GO membrane samples for the FT-IR were prepared with thick GO layers under the same conditions. The *d*-spacings of the GO sheets in the active layer were analyzed by using an X-ray diffractometer (XRD, Panalytical X'Pert Pro, The Netherlands). The scan angles were from 5 to 45°. The step size was 0.5°, and the scan speed was 0.0005°/s. Due to the strong penetration ability of X-rays, the samples for XRD tests were prepared with thick GO layers under the same conditions to obtain clearer signal-to-noise ratios. Raman spectra were recorded with a Renishaw (UK) InVia Raman Microscope using a 633 nm laser. Thermogravimetric analysis (TGA, PerkinElmer Diamond, USA) was used to analyze the mass loss of GO before and after heat treatment (120 °C for 6 h). TGA was carried out under a heating rate of 10 °C/min with a nitrogen flow rate of 20 mL/min. A tensile strength instrument was applied to test the interlayer binding strength of GO membranes. The membrane was tailored into a 0.25 cm^2 square and fixed onto two cylindrical glass holders on the GO side and the porous side using commercial adhesive. The contact area between the membrane and holders were 0.126 cm^2 on each side. The test was conducted at a deformation velocity of 1 mm/min, and the tensile strength as a function of deformation distance was recorded by an interconnected computer.

Separation Performance. The separation performance tests were carried out using a dead-end set (HP4750 STIRRED CELL, Sterlitech, USA) with an effective filtration area of 14.6 cm^2. A series of organic dyes (methyl viologen, methyl red, methylene blue, rose bengal, chrysoidine G, crystal violet, and xylenol orange, 40 ppm aqueous solutions) and two kinds of salts (NaCl and Na_2SO_4, 1000 ppm) were prepared to determine the molecular sieving capability of GO membranes. All of the filtration tests were conducted under 30 psi (equal to 2.07 bar) and operated for 30 min before the permeance data was collected. Each statistical result was obtained by testing at least three independently prepared membranes.

The T-FLO-GO membrane was also tested using a cross-flow system to examine its long-term filtration stability (24 h). The membrane was placed in a stainless-steel cell with an effective area of 17 cm^2 and operated under a constant cross-flow velocity of 14 cm/s. A feed tank was connected to a mechanical pump, which flowed a feed solution (40 ppm methylene blue aqueous solution) across the membrane. A pressure gauge was placed on the feed side of the cell to monitor the input pressure. The output after membrane filtration was monitored with a flow meter, and its' readings were recorded by an interconnected computer. The feed and permeate were collected and further analyzed using UV−vis spectroscopy (PerkinElmer Lambda 20, USA).

The concentrations of the salts were positively correlated with the solution conductivity measured using an XL50 conductivity meter (Fisher Scientific Accumet, USA). The salt rejection was obtained with the followed equation

$$R(\%) = 1 - \frac{\sigma_p}{\sigma_f} \quad (1)$$

where σ_p refers to the conductivity of the permeate and σ_f refers to that of the feed solution. The concentrations of dye solutions were positively correlated with their absorbance by UV−vis spectroscopy (PerkinElmer Lambda 20, USA). The rejection was calculated according to the following equation

$$R(\%) = 1 - \frac{A_p}{A_f} \quad (2)$$

where A_p refers to the absorbance of the permeate and A_f refers to that of the feed solution. The permeability was calculated by a computer connected to a scale that recorded the dynamic mass change of the permeate every 30 s. The membranes were compacted with DI water for 30 min under 30 psi, and the data were recorded when the flux stabilized. The membrane permeability was evaluated using DI water and calculated precisely according to the equation

$$J = \frac{V}{A \cdot t \cdot \triangle P} \quad (3)$$

where J is the permeation flux ($L \cdot m^{-2} \cdot hr^{-1} \cdot bar^{-1}$), V is the volume of the permeate (L) over a certain time t (hr), A is the effective filtration area (m^2), and ΔP is the driving pressure (bars).

■ ASSOCIATED CONTENT

Supporting Information

The Supporting Information is available free of charge at https://pubs.acs.org/doi/10.1021/acs.nanolett.9b03780.

Additional figures and tables as described in the text (PDF)

■ AUTHOR INFORMATION

Corresponding Author

Richard B. Kaner − *Department of Chemistry and Biochemistry and California NanoSystems Institute and Department of Material Science and Engineering, University of California, Los Angeles, Los Angeles, California 90095, United States;* orcid.org/0000-0003-0345-4924; Email: kaner@chem.ucla.edu

Authors

Shuangmei Xue − *Department of Chemistry and Biochemistry and California NanoSystems Institute, University of California, Los Angeles, Los Angeles, California 90095, United States; State Key Laboratory of Chemical Engineering, East China University of Science and Technology, 200237 Shanghai, P. R. China*

Chenhao Ji − *Department of Chemistry and Biochemistry and California NanoSystems Institute, University of California, Los Angeles, Los Angeles, California 90095, United States; State Key Laboratory of Chemical Engineering, East China University of Science and Technology, 200237 Shanghai, P. R. China*

Matthew D. Kowal − *Department of Chemistry and Biochemistry and California NanoSystems Institute, University of California, Los Angeles, Los Angeles, California 90095, United States*

Jenna C. Molas − *Department of Chemistry and Biochemistry and California NanoSystems Institute, University of California, Los Angeles, Los Angeles, California 90095, United States*

Cheng-Wei Lin − *Department of Chemistry and Biochemistry and California NanoSystems Institute, University of California, Los Angeles, Los Angeles, California 90095, United States*

Brian T. McVerry − *Department of Chemistry and Biochemistry and California NanoSystems Institute, University of California, Los Angeles, Los Angeles, California 90095, United States*

https://dx.doi.org/10.1021/acs.nanolett.9b03780
Nano Lett. XXXX, XXX, XXX−XXX

Christopher L. Turner − *Department of Chemistry and Biochemistry and California NanoSystems Institute, University of California, Los Angeles, Los Angeles, California 90095, United States*

Wai H. Mak − *Department of Chemistry and Biochemistry and California NanoSystems Institute, University of California, Los Angeles, Los Angeles, California 90095, United States;* orcid.org/0000-0002-8342-1382

Mackenzie Anderson − *Department of Chemistry and Biochemistry and California NanoSystems Institute, University of California, Los Angeles, Los Angeles, California 90095, United States;* orcid.org/0000-0002-7605-2558

Mit Muni − *Department of Chemistry and Biochemistry and California NanoSystems Institute, University of California, Los Angeles, Los Angeles, California 90095, United States*

Eric M. V. Hoek − *Department of Civil and Environmental Engineering, Institute of the Environment & Sustainability and California NanoSystems Institute, University of California, Los Angeles, Los Angeles, California 90095, United States;* orcid.org/0000-0002-5748-6481

Zhen-Liang Xu − *State Key Laboratory of Chemical Engineering, East China University of Science and Technology, 200237 Shanghai, P. R. China;* orcid.org/0000-0002-1436-4927

Complete contact information is available at: https://pubs.acs.org/10.1021/acs.nanolett.9b03780

Author Contributions

‡S.X. and C.J. contributed equally to this work.

Notes

The authors declare no competing financial interest.

■ ACKNOWLEDGMENTS

The authors thank the China Scholarship Council (S.X. and C.J.), the USA/China Clean Energy Research Center for Water-Energy Technologies (CERC-WET) (R.B.K. and E.M.V.H.), the UC Grand Challenge Program (R.B.K. and E.M.V.H.), and the Dr. Myung Ki Hong Endowed Chair in Materials Innovation (R.B.K.) for financial support. The authors would also like to thank Technical Fibre Products for their generous donation of nonwoven fabrics.

■ REFERENCES

(1) Haase, M. F.; Jeon, H.; Hough, N.; Kim, J. H.; Stebe, K. J.; Lee, D. Multifunctional Nanocomposite Hollow Fiber Membranes by Solvent Transfer Induced Phase Separation. *Nat. Commun.* **2017**, *8*, 1234.

(2) Karan, S.; Jiang, Z.; Livingston, A. G. Sub − 10 nm Polyamide Nanofilms with Ultrafast Solvent Transport for Molecular Separation. *Science* **2015**, *348* (6241), 1347−1352.

(3) Jimenez-Solomon, M. F.; Song, Q.; Jelfs, K. E.; Munoz-Ibanez, M.; Livingston, A. G. Polymer Nanofilms with Enhanced Microporosity by Interfacial Polymerization. *Nat. Mater.* **2016**, *15* (7), 760−767.

(4) Soler-Crespo, R. A.; Gao, W.; Mao, L.; Nguyen, H. T.; Roenbeck, M. R.; Paci, J. T.; Huang, J.; Nguyen, S. T.; Espinosa, H. D. The Role of Water in Mediating Interfacial Adhesion and Shear Strength in Graphene Oxide. *ACS Nano* **2018**, *12*, 6089−6099.

(5) Celebi, K.; Buchheim, J.; Wyss, R. M.; Droudian, A.; Gasser, P.; Shorubalko, I.; Kye, J., II; Lee, C.; Park, H. G. Ultimate Permeation across Atomically Thin Porous Graphene. *Science* **2014**, *344* (6181), 289−292.

(6) Yang, Y.; Yang, X.; Liang, L.; Gao, Y.; Cheng, H.; Li, X.; Zou, M.; Ma, R.; Yuan, Q.; Duan, X. Large-area graphene-nanomesh/carbon-nanotube hybrid membranes for ionic and molecular nanofiltration. *Science* **2019**, *364*, 1057−1062.

(7) Shen, X.; Wang, Z.; Wu, Y.; Liu, X.; He, Y. B.; Zheng, Q.; Yang, Q. H.; Kang, F.; Kim, J. K. A Three-Dimensional Multilayer Graphene Web for Polymer Nanocomposites with Exceptional Transport Properties and Fracture Resistance. *Mater. Horiz.* **2018**, *5* (2), 275−284.

(8) Liu, G.; Jin, W.; Xu, N. Graphene-Based Membranes. *Chem. Soc. Rev.* **2015**, *44* (15), 5016−5030.

(9) Koros, W. J.; Zhang, C. Materials for Next-Generation Molecularly Selective Synthetic Membranes. *Nat. Mater.* **2017**, *16* (3), 289−297.

(10) Ying, W.; Cai, J.; Zhou, K.; Chen, D.; Ying, Y.; Guo, Y.; Kong, X.; Xu, Z.; Peng, X. Ionic Liquid Selectively Facilitates CO2 Transport through Graphene Oxide Membrane. *ACS Nano* **2018**, *12*, 5385−5393.

(11) Singh, S. P.; Li, Y.; Zhang, J.; Tour, J. M.; Arnusch, C. J. Sulfur-Doped Laser-Induced Porous Graphene Derived from Polysulfone-Class Polymers and Membranes. *ACS Nano* **2018**, *12*, 289−297.

(12) Chen, P.; Zhang, M.; Liu, M.; Wong, I.; Hurt, R. H. Ultrastretchable Graphene-Based Molecular Barriers for Chemical Protection, Detection, and Actuation. *ACS Nano* **2018**, *12*, 234−244.

(13) Wang, Y.; Chen, S.; Qiu, L.; Wang, K.; Wang, H.; Simon, G. P.; Li, D. Graphene-Directed Supramolecular Assembly of Multifunctional Polymer Hydrogel Membranes. *Adv. Funct. Mater.* **2015**, *25* (1), 126−133.

(14) Georgakilas, V.; Perman, J. A.; Tucek, J.; Zboril, R. Broad Family of Carbon Nanoallotropes: Classification, Chemistry, and Applications of Fullerenes, Carbon Dots, Nanotubes, Graphene, Nanodiamonds, and Combined Superstructures. *Chem. Rev.* **2015**, *115* (11), 4744−4822.

(15) He, G.; Chang, C.; Xu, M.; Hu, S.; Li, L.; Zhao, J.; Li, Z.; Li, Z.; Yin, Y.; Gang, M.; Wu, H.; Yang, X.; Guiver, M. D.; Jiang, Z. Tunable Nanochannels along Graphene Oxide/Polymer Core-Shell Nanosheets to Enhance Proton Conductivity. *Adv. Funct. Mater.* **2015**, *25* (48), 7502−7511.

(16) Kim, H. W.; Yoon, H. W.; Yoon, S.; Yoo, B. M.; Ahn, B. K.; Cho, Y. H.; Shin, H. J.; Yang, H.; Paik, U.; Kwon, S.; et al. Supplementary Material for Selective Gas Transport Through. *Science* **2013**, *342*, 91−95.

(17) Liu, X.; Tang, C.; Du, X.; Xiong, S.; Xi, S.; Liu, Y.; Shen, X.; Zheng, Q.; Wang, Z.; Wu, Y.; Horner, A.; Kim, J.-K. A Highly Sensitive Graphene Woven Fabric Strain Sensor for Wearable Wireless Musical Instruments. *Mater. Horiz.* **2017**, *4* (3), 477−486.

(18) Huang, K.; Liu, G.; Shen, J.; Chu, Z.; Zhou, H.; Gu, X.; Jin, W.; Xu, N. High-Efficiency Water-Transport Channels Using the Synergistic Effect of a Hydrophilic Polymer and Graphene Oxide Laminates. *Adv. Funct. Mater.* **2015**, *25* (36), 5809−5815.

(19) You, Y.; Sahajwalla, V.; Yoshimura, M.; Joshi, R. K. Graphene and Graphene Oxide for Desalination. *Nanoscale* **2016**, *8* (1), 117−119.

(20) Sun, P.; Wang, K.; Zhu, H. Recent Developments in Graphene-Based Membranes: Structure, Mass-Transport Mechanism and Potential Applications. *Adv. Mater.* **2016**, *28* (12), 2287−2310.

(21) Huang, L.; Li, Y.; Zhou, Q.; Yuan, W.; Shi, G. Graphene Oxide Membranes with Tunable Semipermeability in Organic Solvents. *Adv. Mater.* **2015**, *27* (25), 3797−3802.

(22) Akbari, A.; Sheath, P.; Martin, S. T.; Shinde, D. B.; Shaibani, M.; Banerjee, P. C.; Tkacz, R.; Bhattacharyya, D.; Majumder, M. Large-Area Graphene-Based Nanofiltration Membranes by Shear Alignment of Discotic Nematic Liquid Crystals of Graphene Oxide. *Nat. Commun.* **2016**, *7*, 10891.

(23) Chen, L.; Shi, G.; Shen, J.; Peng, B.; Zhang, B.; Wang, Y.; Bian, F.; Wang, J.; Li, D.; Qian, Z.; Xu, G.; Liu, G.; Zeng, J.; Zhang, L.; Yang, Y.; Zhou, G.; Wu, M.; Jin, W.; Li, J.; Fang, H. Ion Sieving in Graphene Oxide Membranes via Cationic Control of Interlayer Spacing. *Nature* **2017**, *550* (7676), 380.

(24) Nam, Y. T.; Choi, J.; Kang, K. M.; Kim, D. W.; Jung, H. T. Enhanced Stability of Laminated Graphene Oxide Membranes for

https://dx.doi.org/10.1021/acs.nanolett.9b03780
Nano Lett. XXXX, XXX, XXX−XXX

Nanofiltration via Interstitial Amide Bonding. *ACS Appl. Mater. Interfaces* **2016**, *8* (40), 27376−27382.
(25) Woo, J. Y.; Oh, J. H.; Jo, S.; Han, C. Nacre-Mimetic Graphene Oxide/Cross-Linking Agent Composite Films with Superior Mechanical Properties. *ACS Nano* **2019**, *13*, 4522−4529.
(26) McVerry, B.; Anderson, M.; He, N.; Kweon, H.; Ji, C.; Xue, S.; Rao, E.; Lee, C.; Lin, C.-W.; Chen, D.; Jun, D.; Sant, G.; Kaner, R. B. Next-Generation Asymmetric Membranes Using Thin-Film Liftoff. *Nano Lett.* **2019**, *19*, 5036.
(27) Cruz-Silva, R.; Endo, M.; Terrones, M. Graphene Oxide Films, Fibers, and Membranes. *Nanotechnol. Rev.* **2016**, *5* (4), 377−391.
(28) Putz, K. W.; Compton, O. C.; Segar, C.; An, Z.; Nguyen, S. T.; Brinson, L. C. Evolution of Order during Vacuum-Assisted Self-Assembly of Graphene Oxide Paper and Associated Polymer Nanocomposites. *ACS Nano* **2011**, *5* (8), 6601−6609.
(29) Wei, Y.; Zhang, Y.; Gao, X.; Yuan, Y.; Su, B.; Gao, C. Declining Flux and Narrowing Nanochannels under Wrinkles of Compacted Graphene Oxide Nanofiltration Membranes. *Carbon* **2016**, *108*, 568−575.
(30) Yang, Q.; Su, Y.; Chi, C.; Cherian, C. T.; Huang, K.; Kravets, V. G.; Wang, F. C.; Zhang, J. C.; Pratt, A.; Grigorenko, A. N.; Guinea, F.; Geim, A. K.; Nair, R. R. Ultrathin Graphene-Based Membrane with Precise Molecular Sieving and Ultrafast Solvent Permeation. *Nat. Mater.* **2017**, *16* (12), 1198−1202.
(31) Saraswat, V.; Jacobberger, R. M.; Ostrander, J. S.; Hummell, C. L.; Way, A. J.; Wang, J.; Zanni, M. T.; Arnold, M. S. Invariance of Water Permeance through Size-Differentiated Graphene Oxide Laminates. *ACS Nano* **2018**, *12*, 7855−7865.
(32) Chua, C. K.; Pumera, M. Chemical Reduction of Graphene Oxide: A Synthetic Chemistry Viewpoint. *Chem. Soc. Rev.* **2014**, *43* (1), 291−312.
(33) Surwade, S. P.; Smirnov, S. N.; Vlassiouk, I. V.; Unocic, R. R.; Veith, G. M.; Dai, S.; Mahurin, S. M. Water Desalination Using Nanoporous Single-Layer Graphene. *Nat. Nanotechnol.* **2015**, *10* (5), 459−464.
(34) Wang, L.; Drahushuk, L. W.; Cantley, L.; Koenig, S. P.; Liu, X.; Pellegrino, J.; Strano, M. S.; Scott Bunch, J. Molecular Valves for Controlling Gas Phase Transport Made from Discrete Ångström-Sized Pores in Graphene. *Nat. Nanotechnol.* **2015**, *10* (9), 785−790.
(35) Jain, T.; Rasera, B. C.; Guerrero, R. J. S.; Boutilier, M. S. H.; O'Hern, S. C.; Idrobo, J. C.; Karnik, R. Heterogeneous Sub-Continuum Ionic Transport in Statistically Isolated Graphene Nanopores. *Nat. Nanotechnol.* **2015**, *10* (12), 1053−1057.
(36) Abraham, J.; Vasu, K. S.; Williams, C. D.; Gopinadhan, K.; Su, Y.; Cherian, C. T.; Dix, J.; Prestat, E.; Haigh, S. J.; Grigorieva, I. V.; Carbone, P.; Geim, A. K.; Nair, R. R. Tunable Sieving of Ions Using Graphene Oxide Membranes. *Nat. Nanotechnol.* **2017**, *12* (6), 546−550.
(37) Han, Y.; Xu, Z.; Gao, C. Ultrathin Graphene Nanofiltration Membrane for Water Purification. *Adv. Funct. Mater.* **2013**, *23* (29), 3693−3700.
(38) Huang, L.; Chen, J.; Gao, T.; Zhang, M.; Li, Y.; Dai, L.; Qu, L.; Shi, G. Reduced Graphene Oxide Membranes for Ultrafast Organic Solvent Nanofiltration. *Adv. Mater.* **2016**, *28* (39), 8669−8674.

https://dx.doi.org/10.1021/acs.nanolett.9b03780
Nano Lett. XXXX, XXX, XXX−XXX